Available online at www.sciencedirect.com

ScienceDirect

Procedia CIRP 24 (2014) 74 – 79

www.elsevier.com/locate/procedia

New Production Technologies in Aerospace Industry - 5th Machining Innovations Conference (MIC 2014)

# A Mechanistic Approach to Model Cutting Forces in Drilling with Indexable Inserts

Amir Parsian[a,b,*], Martin Magnevall[a], Tomas Beno[b], Mahdi Eynian[b]

[a]*AB Sandvik Coromant, SE-811 81 Sandviken, Sweden*

[b]*University West, SE-461 86 Trollhättan, Sweden*

* Corresponding author. Tel.: +46(0)723111844.*E-mail address:*amir.parsian@sandvik.com

**Abstract**

Holes are made in many industrial parts that need screws, pins or channels for passing fluids. The general method to produce holes in metal cutting is by drilling operations. Indexable insert drills are often used to make short holes at a low cost. However, indexable drills are prone to vibrate under certain circumstances, causing vibrations that affect tool life. Therefore, a good prediction of cutting-forces in drilling is important to get a good description of the cutting process for optimization of tool body and insert design. Reliable simulations of dynamic forces also aid in prediction of chatter vibrations that have significant effects on the quality of the manufactured parts as well as the tool life. In this paper, a mechanistic approach is used to model the cutting-forces. Cutting-force coefficients are identified from measured instantaneous forces in drilling operations. These coefficients are used for simulating torque around drill-axis, axial force and cutting-forces in the plane perpendicular to drill-axis. The forces are modeled separately for peripheral and central insert, which results in a detailed description of the cutting-forces acting on each insert. The forces acting on each insert are estimated by dividing the cutting edges into small segments and the cutting-forces acting on each segment are calculated. The total forces are predicted by summation of the forces acting on each segment. Simulated torque and forces are compared to measured cutting-forces for two different feeds. A good agreement between predicted and experimental results, especially in torque and axial-force, is observed.



Selection and peer-review under responsibility of the International Scientific Committee of the "New Production Technologies in Aerospace Industry" conference in the person of the Conference Chairs: Prof. Berend Denkena, Prof. Yusuf Altintas, Prof. Pedro J. Arrazola, Prof. Tojiro Aoyama and Prof. Dragos Axinte

*Keywords:*Indexable insert drill; Cutting-forces; Mechanistic force model.

## 1. Introduction

Drilling operations are done on many industrial parts. Depending on size of holes, workpiece material and cutting conditions, different types of drill might be used. Indexable insert drills use two or more inserts to make holes, the majority of indexable drills have two inserts. While one insert is cutting the center, the second insert cut the peripheral part of the hole. Usually, these two inserts are not identical, both edge geometry and coating can differ since they operate at different average cutting speeds and under different specific load conditions. Thus, each insert has its own mechanistic cutting-force coefficients.

A good prediction of cutting-forces aids in the product development process and facilitates improved tool designs, improved cutting process and increased productivity.

Different methods have been used to predict cutting-forces in drilling and can be found in [1-9]. A comprehensive work on mechanics and dynamics of drilling is found in [3]. In [5] a finite element method is applied to predict thrust force and torque in drilling. The technique is validated by experimental data. Finite element modeling offers a good approach to predict cutting-forces. However, due to computational time it



Selection and peer-review under responsibility of the International Scientific Committee of the "New Production Technologies in Aerospace Industry" conference in the person of the Conference Chairs: Prof. Berend Denkena, Prof. Yusuf Altintas, Prof. Pedro J. Arrazola, Prof. Tojiro Aoyama and Prof. Dragos Axinte
doi:10.1016/j.procir.2014.07.138

can be a costly approach for optimization purposes. A unified method is presented in [2] to predict cutting-forces in different metal cutting operations. The modeling process in [2] starts with obtaining shear stress, shear angle and friction angle from orthogonal tests and transforming forces into other coordinate systems such as the machine tool coordinates. To obtain cutting-force coefficients, a set of turning operations at different feeds for each insert is required. Practically this can be time consuming and costly.

This paper proposes a method to model cutting-forces by applying different specific cutting-force coefficients for each insert. In this work, the method developed in [2] is used to predict cutting-forces for each element on cutting edge. However, the main difference is that cutting-force coefficients are obtained directly from drilling based on experimental tests from a rotating force dynamometer. This approach is faster and less costly because there is no need for preparing tool holders and workpiece for turning operations.

The type of tools studied in this work is an indexable insert drill with two inserts. The suggested method shows how to model cutting-forces for indexable drills by combining experimental tests and simulations. Structural vibrations and bending of the tool are not considered in the model.

**Nomenclature**

| | |
|---|---|
| $\Delta F_u^i, \Delta F_v^i$ | Segmental force in friction and normal directions |
| $\Delta F_t^i, \Delta F_f^i$ | Segmental force in tangential and feed directions |
| $\Delta F_x^i, \Delta F_y^i, \Delta F_z^i$ | Segmental force in $x, y$ and $z$ directions |
| $F_x, F_y, F_z$ | Total force in $x, y$ and $z$ directions |
| M | Total torque around the drill-axis |
| $\Delta M^i$ | Segmental torque |
| $\alpha^i$ | Angle between cutting edge and $z$ direction |
| $\beta^i$ | Angle between $\Delta F_t^i$ and negative $y$-axis |
| $L^i$ | Length of cutting edge for segment $i$ |
| $\Gamma^i$ | Rake angle for segment $i$ |
| $h^i$ | Uncut chip thickness for segment $i$ |
| $r^i$ | Average distance between segment $i$ and drill-axis |
| $f_n$ | Axial feed |
| $K_{tc}^C, K_{fc}^C$ | Tangential and feed cutting-force coefficients for central insert |
| $K_{tc}^P, K_{fc}^P$ | Tangential and feed cutting-force coefficients for peripheral insert |
| $K_{te}^C, K_{fe}^C$ | Edge-coefficients for tangential and feed cutting-forces for central insert |
| $K_{te}^P, K_{fe}^P$ | Edge-coefficients for tangential and feed cutting-forces for peripheral insert |
| $K_{uc}^C, K_{vc}^C$ | Friction and normal cutting-force coefficients for central insert |
| $K_{uc}^P, K_{vc}^P$ | Friction and normal cutting-force coefficients for peripheral insert |
| $K_{ue}^C, K_{ve}^C$ | Edge-coefficients for friction and normal cutting-forces for central insert |
| $K_{ue}^P, K_{ve}^P$ | Edge-coefficients for friction and normal cutting-forces for peripheral insert |

## 2. Theory

By using different cutting-force coefficients for central and peripheral inserts and applying a linear relationship between cutting-forces and uncut chip thickness, it is possible to obtain a good estimation for the torque and the thrust force as well as cutting-forces in the plane perpendicular to the drill-axis.

In this work, it is assumed that the cutting edges are perpendicular to the cutting speed direction. The basic principle used to estimate the cutting-forces is to divide each insert edge into small segments, then identify which segments are engaged in the workpiece and calculate the directional force components for each segment. The cutting-forces acting on the individual segments are assumed to be orthogonal (friction and normal forces, $\Delta F_u^i$ and $\Delta F_v^i$, respectively) as shown in Figure 1.

A right-hand global coordinate system $(x, y, z)$ is defined with $z$ along drill-axis (see Figure 2 and Figure 3).The total directional cutting-forces are then obtained by transformation into global coordinates $(x, y, z)$, Figure 2, and summation of the forces acting on each individual segment. In Figure 2, $\Delta F_f^i$ and $\Delta F_z^i$ are in the same plane and perpendicular to $\Delta F_t^i$.

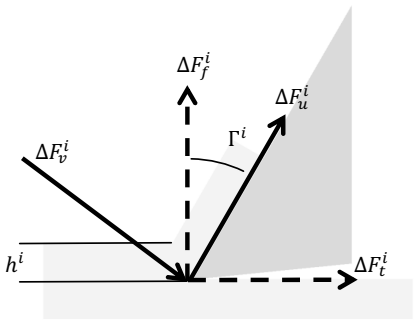


Figure 1.Segmental friction force ($\Delta F_u^i$) and normal force ($\Delta F_v^i$) are transformed into tangential ($\Delta F_t^i$) and feed ($\Delta F_f^i$) directions. $h^i$is uncut chip thickness and $\Gamma^i$ is rake angle for segment $i$.

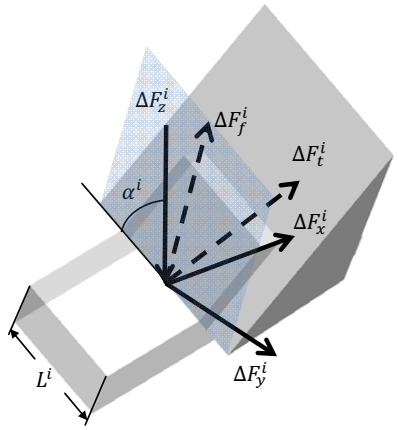


Figure 2.Segmental cutting-forces shown in global coordinates ($\Delta F_x^i$, $\Delta F_y^i$, $\Delta F_z^i$). $L^i$ is the length of the segmental cutting edge. $\Delta F_t^i$ and $\Delta F_f^i$ are segmental cutting-force in tangential and feed directions, respectively.

The global coordinates $(x, y, z)$ are not stationary and

rotate as the drill rotates. $x$ is parallel to the cutting edge of peripheral insert, $z$ is along the drill-axis and $y$ is perpendicular to $x$ and $z$. The tool is assumed to rotate counter-clockwise. The following part provides a detailed description of the method.

Positions and cutting edges' profiles of peripheral and central inserts are shown in Figure 3 and Figure 4. Product codes for the inserts and tool-body are listed in Table 1.

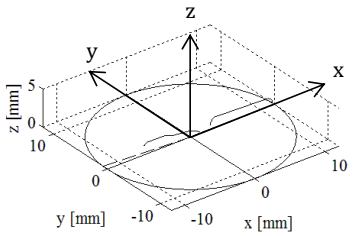


Figure 3. Positions of inserts after installation on the body. Global coordinate system (x, y, z) is a rotating coordinate system. $x$ is parallel to the cutting edge of peripheral insert and z is along the drill-axis.

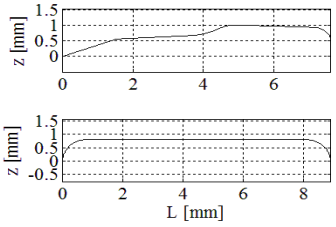


Figure 4. Edges' profile for central insert (top) and peripheral insert (bottom).

Table 1. Product codes for tool-body and inserts used in the paper.

| Item | Product's code |
|---|---|
| Tool-body | 880-D2400L25-04 |
| Central-Insert | 880-0503…-C |
| Peripheral-Insert | 880-0503…-P |

$\Delta F_u^i$ and $\Delta F_v^i$ (see Figure 1) are obtained by Equations (1) and (2) [2].

$$\Delta F_u^i = K_{uc} \cdot h^i \cdot L^i + K_{ue} \cdot L^i \quad (1)$$

$$\Delta F_v^i = K_{vc} \cdot h^i \cdot L^i + K_{ve} \cdot L^i \quad (2)$$

$K_{uc}$ and $K_{vc}$ are friction and normal cutting-force coefficients. $K_{ue}$ and $K_{ve}$ are friction and normal edge force coefficients [2].

In the above equations, $\Delta F_u^i$ and , $\Delta F_v^i$ are segmental friction and normal force, respectively. $L^i$ is the cutting edge length and $h^i$ is uncut chip thickness for segment $i$. $h^i$ is calculated as:

$$h^i = f_n \cdot \sin(\alpha^i) \quad (3)$$

Where $\alpha^i$ is the angle between the cutting edge and the drill-axis (see Figure 2), and $f_n$ refers to feed per revolution.

Putting Equations (1) and (2) in matrix form yields:

$$\begin{bmatrix} \Delta F_u^i \\ \Delta F_v^i \end{bmatrix} = L^i \begin{bmatrix} K_{uc} & K_{ue} \\ K_{vc} & K_{ve} \end{bmatrix} \begin{bmatrix} h^i \\ 1 \end{bmatrix} \quad (4)$$

From Figure 1, $\Delta F_f^i$ and $\Delta F_t^i$ are found as:

$$\begin{bmatrix} \Delta F_f^i \\ \Delta F_t^i \end{bmatrix} = \begin{bmatrix} \cos(\Gamma^i) & -\sin(\Gamma^i) \\ \sin(\Gamma^i) & \cos(\Gamma^i) \end{bmatrix} \begin{bmatrix} \Delta F_u^i \\ \Delta F_v^i \end{bmatrix} \quad (5)$$

$\Gamma^i$ is rake angle for segment $i$.Combining Equations (4) and (5) yields:

$$\begin{bmatrix} \Delta F_f^i \\ \Delta F_t^i \end{bmatrix} = L^i \begin{bmatrix} \mathrm{K_{fc}} & \mathrm{K_{fe}} \\ \mathrm{K_{tc}} & \mathrm{K_{te}} \end{bmatrix} \begin{bmatrix} h^i \\ 1 \end{bmatrix} \quad (6)$$

Where,

$$\begin{bmatrix} \mathrm{K_{fc}} & \mathrm{K_{fe}} \\ \mathrm{K_{tc}} & \mathrm{K_{te}} \end{bmatrix} = \begin{bmatrix} \cos(\Gamma^i) & -\sin(\Gamma^i) \\ \sin(\Gamma^i) & \cos(\Gamma^i) \end{bmatrix} \begin{bmatrix} K_{uc} & K_{ue} \\ K_{vc} & K_{ve} \end{bmatrix} \quad (7)$$

$K_{tc}$ and $K_{fc}$ are tangential and feed cutting-force coefficients. $K_{te}$ and $K_{fe}$ are tangential and feed-edge force coefficients.

The tangential force components, $\Delta F_t^i$, can be related to torque as:

$$\Delta M^i = \Delta F_t^i \cdot r^i \quad (8)$$

$r^i$ is average distance between segment $i$ and the drill-axis. The total torque is calculated as:

$$M = \Sigma \Delta M^i = \Sigma \left( \Delta F_t^i r^i \right) \quad (9)$$

Combining Equations (3), (6) and (9) yields:

$$M = f_n \cdot K_{tc} \Sigma L^i \sin(\alpha^i)\, r^i + K_{te} \Sigma L^i r^i \quad (10)$$

Equation (10) can be expressed as:

$$M = a_M \cdot f_n + b_M \quad (11)$$

Where $a_M$ and$b_M$ are given in Equation (18).

As shown by Figure 2 and Figure 5, forces in x, y and z directions acting on each individual segment are calculated as:

$$\Delta F_z^i = -\Delta F_i^f \cdot \sin(\alpha^i) \quad (12)$$

$$\Delta F_x^i = \sin(\beta^i) \Delta F_t^i + \cos(\beta^i) cos(\alpha^i) \Delta F_f^i \quad (13)$$

$$\Delta F_y^i = -\cos(\beta^i)\, \Delta F_t^i + \sin(\beta^i) \cos(\alpha^i)\, \Delta F_f^i \quad (14)$$

Where $\beta^i$ is the angle between $\Delta F_t^i$and negative $y$-axis, Figure 5.

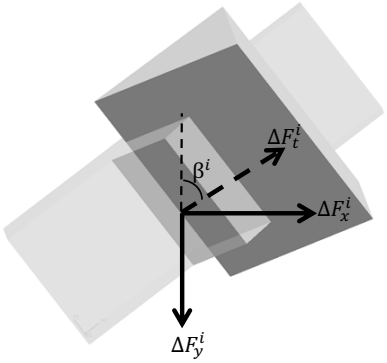


Figure 5. Segmental cutting-forces shown in global coordinates ($\Delta F_x^i$, $\Delta F_y^i$). $\beta^i$ is the angle between $\Delta F_t^i$ and negative $y$-axis. $\Delta F_t^i$, $\Delta F_x^i$ and $\Delta F_y^i$ are in the same plane.

Combining Equations (6) and (12)-(14) and summing up the individual force components yields:

$$F_z = a_z \cdot f_n + b_z \tag{15}$$
$$F_x = a_x \cdot f_n + b_x \tag{16}$$
$$F_y = a_y \cdot f_n + b_y \tag{17}$$

Where $a_z$, $b_z$, $a_x$, $b_x$, $a_y$ and $b_y$ can be expressed as:

$$\begin{aligned}
a_M &= K_{tc}^C C_{11} + K_{tc}^P C_{12} \\
b_M &= K_{te}^C C_{23} + K_{te}^P c_{24} \\
a_z &= K_{fc}^C C_{35} + K_{fc}^P C_{36} \\
b_z &= K_{fe}^C C_{47} + K_{fe}^P C_{48} \\
a_x &= K_{tc}^C C_{51} + K_{fc}^C C_{55} + K_{tc}^P C_{52} + K_{fc}^P C_{56} \\
b_x &= K_{te}^C C_{63} + K_{fe}^C C_{67} + K_{te}^P C_{64} + K_{fe}^P C_{68} \\
a_y &= K_{tc}^C C_{71} + K_{fc}^C C_{75} + K_{tc}^P C_{72} + K_{fc}^P C_{76} \\
b_y &= K_{te}^C C_{83} + K_{fe}^C C_{87} + K_{te}^P C_{84} + K_{fe}^P C_{88}
\end{aligned} \tag{18}$$

The $C_{mn}$ elements in Equation (18) are shown in Equation (21). Subscripts $m$ and $n$ refer to matrix position row and column, respectively. Superscripts $C$ and $P$ refer to central and peripheral inserts, respectively. $i \in C$ refers to segment $i$ on the central-insert and $i \in P$ refers to segment $i$ on the peripheral-insert.

Equation (18) in a matrix form is rewritten as:

$$[\boldsymbol{C}]_{\boldsymbol{8\times 8}} \cdot [\boldsymbol{A}]_{\boldsymbol{8\times 1}} = [\boldsymbol{B}]_{\boldsymbol{8\times 1}} \tag{19}$$

Where vectors $[\boldsymbol{A}]$ and $[\boldsymbol{B}]$ are:

$$\begin{aligned}
[\boldsymbol{A}] &= \begin{bmatrix} K_{tc}^C & K_{tc}^P & K_{te}^C & K_{te}^P & K_{fc}^C & K_{fc}^P & K_{fe}^C & K_{fe}^P \end{bmatrix}^T \\
[\boldsymbol{B}] &= \begin{bmatrix} a_M & b_M & a_z & b_z & a_x & b_x & a_y & b_y \end{bmatrix}^T
\end{aligned} \tag{20}$$

Equation (21) shows the nonzero elements of matrix $[\boldsymbol{C}]$.

It should be noted that thrust-force has a magnitude equal to $F_z$ and it is in the negative z-axis.

Equation (19) is a system of linear equations that makes a relationship between cutting-force coefficients ($[\boldsymbol{A}]$), cutting-forces ($[\boldsymbol{B}]$) and tool-geometry ($[\boldsymbol{C}]$).

$$\begin{aligned}
C_{11} &= \textstyle\sum_{i\in C} L^i \sin(\alpha^i)\, r^i \\
C_{12} &= \textstyle\sum_{i\in P} L^i \sin(\alpha^i)\, r^i \\
C_{23} &= \textstyle\sum_{i\in C} L^i r^i \\
C_{24} &= \textstyle\sum_{i\in P} L^i r^i \\
C_{35} &= -\textstyle\sum_{i\in C} L^i \sin(\alpha^i) \sin(\alpha^i) \\
C_{36} &= -\textstyle\sum_{i\in P} L^i \sin(\alpha^i) \sin(\alpha^i) \\
C_{47} &= -\textstyle\sum_{i\in C} L^i \sin(\alpha^i) \\
C_{48} &= -\textstyle\sum_{i\in P} L^i \sin(\alpha^i) \\
C_{51} &= \textstyle\sum_{i\in C} L^i \sin(\alpha^i) \sin(\beta^i) \\
C_{52} &= \textstyle\sum_{i\in P} L^i \sin(\alpha^i) \sin(\beta^i) \\
C_{55} &= \textstyle\sum_{i\in C} L^i \sin(\alpha^i) \cos(\alpha^i) \cos(\beta^i) \\
C_{56} &= \textstyle\sum_{i\in P} L^i \sin(\alpha^i) \cos(\alpha^i) \cos(\beta^i) \\
C_{63} &= \textstyle\sum_{i\in C} L^i \sin(\beta^i) \\
C_{64} &= \textstyle\sum_{i\in P} L^i \sin(\beta^i) \\
C_{67} &= \textstyle\sum_{i\in C} L^i \cos(\alpha^i) \cos(\beta^i) \\
C_{68} &= \textstyle\sum_{i\in P} L^i \cos(\alpha^i) \cos(\beta^i) \\
C_{71} &= -\textstyle\sum_{i\in C} L^i \sin(\alpha^i) \cos(\beta^i) \\
C_{72} &= -\textstyle\sum_{i\in P} L^i \sin(\alpha^i) \cos(\beta^i) \\
C_{75} &= \textstyle\sum_{i\in C} L^i \sin(\alpha^i) \cos(\alpha^i) \sin(\beta^i) \\
C_{76} &= \textstyle\sum_{i\in P} L^i \sin(\alpha^i) \cos(\alpha^i) \sin(\beta^i) \\
C_{83} &= -\textstyle\sum_{i\in C} L^i \cos(\beta^i) \\
C_{84} &= -\textstyle\sum_{i\in P} L^i \cos(\beta^i) \\
C_{87} &= \textstyle\sum_{i\in C} L^i \cos(\alpha^i) \sin(\beta^i) \\
C_{88} &= \textstyle\sum_{i\in P} L^i \cos(\alpha^i) \sin(\beta^i)
\end{aligned} \tag{21}$$

## 3. Experimental tests and results

A set of experiments were conducted to measure the cutting-forces in global coordinate system $(x, y, z)$ and torque around $z$-axis. A Sandvik Coromant CoroDrill® 880 with a diameter of 24 $[mm]$ was mounted on a rotating force dynamometer to measure the cutting-forces, which results in the global coordinate system $(x, y, z)$ rotating as the drill rotates. The product codes for the tool-body and the inserts are given in Table 1. During the tests, the cutting-speed was held constant. Cutting parameters and material code are given in Table 2.

Table 2. Cutting parameters and material code that were used in the experiments.

| Parameter | Value |
|---|---|
| Cutting speed | 200 $[m/min]$ |
| Feed-rates | 0.1,0.11,0.12,0.13,0.14 $[mm/rev]$ |
| Material | $SS$ 2244 |

For each feed-rate, the average cutting-forces, when the tool was in full engagement, were calculated from measured forces in $x$, $y$ and $z$ directions. Additionally, average torque around the $z$-axis for each feed-rate was obtained from measured torque.

These average values and their linear regressions are shown in Figures 6-9. The elements of $[\boldsymbol{B}]$, Equation (20), are obtained by using Equations (11) and (15)-(17) and comparing them with the obtained linear regressions of the cutting-forces. The elements of $[\boldsymbol{C}]$ are calculated by putting tool and inserts' geometries into Equation (21).

By calculating the elements of matrices $[\boldsymbol{B}]$and $[\boldsymbol{C}]$, and using Equation (19), the elements in $[\boldsymbol{A}]$ can be estimated. By substituting elements of matrix $[\boldsymbol{A}]$ in Equation (7), values for

cutting coefficients for friction and normal forces on each insert are obtained. The estimated values are given in Table 3.

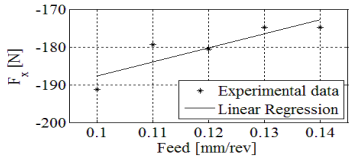


Figure 6. Forces in x-direction versus feed. Cutting speed is 200 [m/min].

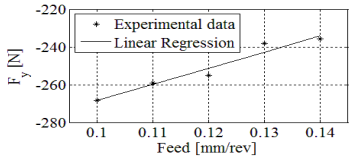


Figure 7. Forces in y-direction versus feed. Cutting speed is 200 [m/min].

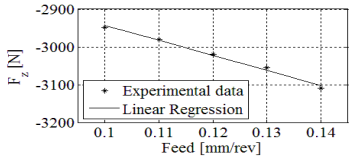


Figure 8. Forces in z-direction versus feed. Cutting speed is 200 [m/min].

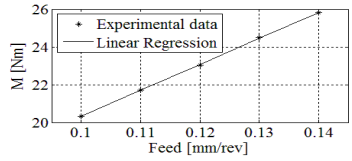


Figure 9. Torque around $z$-axis versus feed. Cutting speed is 200 [m/min].

Table 3. Obtained cutting-force coefficients.

| Cutting-force coefficient | Value |
|---|---|
| $K_{vc}^{C}$ [N/mm$^2$] | 1898.4 |
| $K_{vc}^{P}$[N/mm$^2$] | 1845.4 |
| $K_{ve}^{C}$[N/mm] | 40.1 |
| $K_{ve}^{P}$[N/mm] | 81.8 |
| $K_{uc}^{C}$[N/mm$^2$] | 174.8 |
| $K_{uc}^{P}$[N/mm$^2$] | 681.5 |
| $K_{ue}^{C}$[N/mm] | 241.4 |
| $K_{ue}^{P}$[N/mm] | 187.0 |

The obtained cutting-force coefficients, Table 3, are used to predict cutting-forces. Since the forces are calculated for each segment on the cutting edges, it is possible predict cutting-forces when the tool is partially engaged, for example during entry of holes. Figure 10-Figure 17 show cutting-force simulations compared to measurement results for feed rates of $0.1\ [mm/rev]$ and $0.15\ [mm/rev]$ and cutting speed of $200\ [m/min]$ . The simulation procedure consists of following steps:

- Use axial feed, cutting speed (Table 2) and tool's geometries (Figure 3, Figure 4 and Table 1) to predict which segments are engaged in cutting at each time-step.
- Calculate segmental torque and forces by using obtained cutting-force coefficients (Table 3) and Equations (8), (12), (13) and (14).
- Sum up the segmental torques and forces to obtain the total torque and forces in each direction at each time-step.

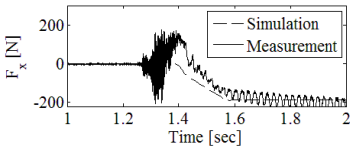


Figure 10. $F_x$ at entry of the hole, feed rate 0.1 [mm/rev] and cutting speed 200 [m/min].The simulation and measurement results do not match well at entry. However, after full engagement, the simulation closely matches the measurement result.

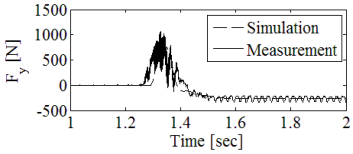


Figure 11. $F_y$ at entry of the hole, feed rate 0.1 [mm/rev] and cutting speed 200 [m/min]. The simulation closely matches the measurement result.

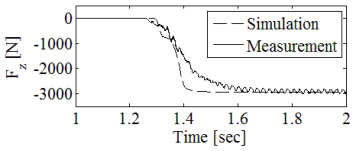


Figure 12. $F_z$ at entry of the hole, feed rate 0.1 [mm/rev] and cutting speed 200 [m/min].The simulation closely matches the measurement result.

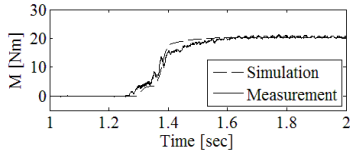


Figure 13. M at entry of the hole, feed rate 0.1 [mm/rev] and cutting speed 200 [m/min]. The simulation closely matches the measurement result.

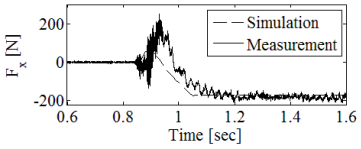


Figure 14. $F_x$ at entry of the hole, feed rate 0.15 [mm/rev] and cutting speed 200 [m/min].The simulation and measurement results do not match well at entry. However, after full engagement, the simulation closely matches the measurement result.

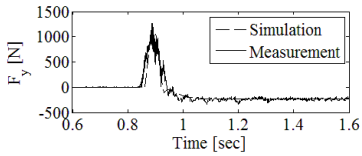


Figure 15. $F_y$ at entry of the hole, feed rate 0.15 [mm/rev] and cutting speed 200 [m/min]. The simulation closely matches the measurement result.

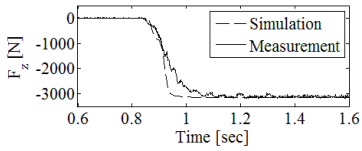


Figure 16. $F_z$ at entry of the hole, feed rate 0.15 [mm/rev] and cutting speed 200 [m/min]. The simulation closely matches the measurement result.

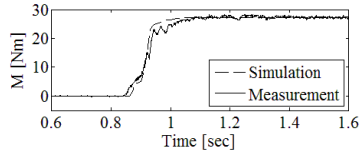


Figure 17. M at entry of the hole, feed rate 0.15 [mm/rev] and cutting speed 200 [m/min]. The simulation closely matches the measurement result.

## 4. Conclusion

A model offered to predict cutting-forces in drilling with indexable insert drills. A new method to obtain mechanistic cutting-force coefficients for two fluted indexable insert drills has been presented. The method identifies separate coefficients for the central and peripheral inserts. The derived cutting coefficients were used to simulate cutting-forces.

The offered method allows identifying cutting-force coefficients directly by measuring cutting-forces in drilling of a few holes. This is usually faster and less costly in comparison to obtaining cutting-force coefficients from orthogonal cutting tests.

In addition, segmental calculation makes it possible to predict cutting-forces at entry of the hole, when inserts are not fully engaged.

Comparison showed a good agreement between simulation and experimental results in $y$-driction and $z$-direction as well as torque. The predictions in $x$-direction during entry of the tool differ compared with the measurements. The reason for this is currently being investigated. However, during full engagement, the model predicts the true cutting-forces and torque well.

## Acknowledgement

Funding of the project provided by AB Sandvik Coromant is gratefully acknowledged.

## References

[1] Altintas Y. Manufacturing Automation: Metal Cutting Mechanics, Machine Tool Vibrations, and CNC Design: Cambridge University Press; 2000.

[2] Kaymakci M, Kilic ZM, Altintas Y. Unified cutting force model for turning, boring, drilling and milling operations. International Journal of Machine Tools & Manufacture. 2012; 54-55: p. 34-45.

[3] Roukema JC. Mechanics and Dynamics of Drilling. PhD [dissertation].The University of British Columbia; 2006.

[4] Ahmadi K, Altintas Y. Stability of lateral, torsional and axial vibrations in drilling. International Journal of Machine Tools & Manufacture. 2013; 68: p. 63-74.

[5] Strenkowski JS, Hsieh CC, Shih AJ. An analytical finite element technique for predicting thrust force and torque in drilling. International Journal of Machine Tools and Manufacture. 2004; 44(12-13): p. 1413-1421.

[6] Stephenson DA, Agapiou JS. Calculation of main cutting edge forces and torque for drills with arbitrary point geometries. International Journal of Machine Tools and Manufacture. 1992; 32(4): p. 521-538.

[7] Armarego JA, Wright JD. Predictive Models for Drilling Thrust and Torque — a comparison of three Flank Configurations. CIRP Annals-Manufacturing Technology. 1984; 33(1): p. 5-10.

[8] Ehmann KF, Kapoor SG, DeVor RE, Lazoglu I. Machining Process Modeling: A review. Journal of Manufacturing Science and Engineering. 1997 November; 119: p. 655-663.

[9] Elhachimi M, Torbaty S, Joyot P. Mechanical modelling of high speed drilling. 1: predicting torque and thrust. International Journal of Machine Tools and Manufacture. 1999; 39(4): p. 553-568.